The 9th German-Japanese Seminar
Nonlinear Problems in Dynamical Systems
—Theory and Applications—
Straelen, Germany, August 20–23, 2000

Efficient Modeling of Rigid-Body Impacts Between Cylinder End Faces Using the Regularized Approach

Andrés Kecskeméthy

Christian Lange, Gerald Grabner

Institut für Mechanik und Getriebelehre,
Technische Universität Graz

Abstract. In this paper, impact effects between cylinder end faces are investigated based on a detailed analysis of the geometric relationships for the different contact situations edge-edge, edge-face, and face-face. The corresponding impact effects are regarded by replacing the (rigid) contact point by a spring with line of action collinear to the main direction of penetration. An empirical blending formulae for providing smooth transition from one contact situation to the other, e.g., from point contact to flat contact, is presented. As an application example, the developed formulas are applied to the modeling and simulation of the inter-vertebral motion of the C5–C6 human cervical spine vertebrae pair, using cylinder-cylinder pairs to represent the facet joints. The application shows good agreement with experimental data, yielding an efficiency boost by a factor of 350 compared to the hyper-ellipsoid approach used in the commercial program MADYMO.

1 Impact Analysis

Let there by two cylinders approaching each other with their faces oriented towards them. In this setting, four possible contact situations can occur: (1) the edge of the upper cylinder touches the flat end of the lower cylinder (Fig. 1); (2) the edge of the upper cylinder touches the egde of the lower cylinder (Fig. 9, right top); (3) the edge of the lower cylinder touches the flat end of the upper cylinder (Fig. 2); and (4) both flat ends of the cylinders rest flatly upon each other (not shown). In order to derive the corresponding equations, skew and flat contact are treated separately, as explained below.

1.1 Skew Contact

Skew contact occurs when the angle between the faces of the colliding cylinders is finite. For this case, three different contact configurations may occur: (case 1) contact of the edge of disc 1 on the face of disc 2 (Fig. 1); (case 2) contact of the edge of disc 2 on

the face of disc 1 (Fig. 2); (case 3) contact of the edge of disc 1 with the edge of disc 2 (Fig. 9, right top).

For case (1), the position vector $\boldsymbol{\rho}_2$ from the center C_2 of disc 2 to the contact point can be written as

$$\boldsymbol{\rho}_2 = -\mathbf{c} + r_1\,\mathbf{u}_{a1} \quad , \tag{1}$$

where $\mathbf{c} = \mathbf{c}_2 - \mathbf{c}_1$ connects the center C_1 of disc 1 with C_2, and r_1 is the radius of disc 1. $\mathbf{u}_{a1}$ denotes the unit vector perpendicular to the line of intersection l of the two disc planes π_1 and π_2 with line of action passing through C_1. Denoting the unit vectors normal to the cylinder faces 1 and 2, respectively, as $\mathbf{n}_1$ and $\mathbf{n}_2$, and setting

$$\mathbf{u} = \frac{\mathbf{n}_1 \times \mathbf{n}_2}{\|\mathbf{n}_1 \times \mathbf{n}_2\|} \quad ,$$

it follows

$$\mathbf{u}_{a1} = \mathbf{n}_1 \times \mathbf{u} \quad .$$

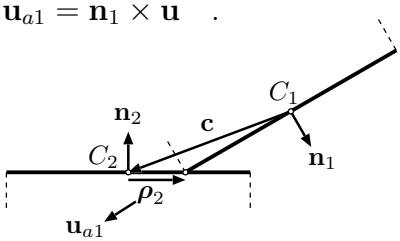

Figure 1: Contact on disc 2.

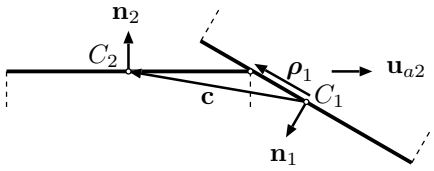

Figure 2: Contact on disc 1.

When contact of the edge of disc 2 on the face of disc 1 (case 2) occurs, the position vector $\boldsymbol{\rho}_1$ pointing from the center of disc 1 to the contact point becomes

$$\boldsymbol{\rho}_1 = \mathbf{c} + r_2\,\mathbf{u}_{a2} \quad , \tag{2}$$

where r_2 is the radius of disc 2 and $\mathbf{u}_{a2}$ is the unit vector perpendicular to the common line of intersection with line of action passing through C_2,

$$\mathbf{u}_{a2} = -\mathbf{n}_2 \times \mathbf{u} \quad .$$

Contact takes place whenever $\|\boldsymbol{\rho}_2\| < r_2$ (case 1) or $\|\boldsymbol{\rho}_1\| < r_1$ (case 2). In order to simulate impact using a regularized approach, the neighborhood of the contact point is regarded as compliant. The corresponding penetration d is defined as acting normal to the face of the cylinder onto which the edge of the other rests. One hence obtains

$$d = \begin{cases} -\mathbf{c}\cdot\mathbf{n}_2 - r_1 \sin\alpha & : \quad \text{case 1} \\ \mathbf{c}\cdot\mathbf{n}_1 - r_2 \sin\alpha & : \quad \text{case 2} \end{cases} \quad .$$

The resulting contact force is normal to this face with magnitude equal to a user-defined stiffness coefficient multiplied by the penetration d, i.e., a virtual linear spring element is attached between the edge of the one cylinder and the face of the other at the contact point with line of action normal to the cylinder face described above.

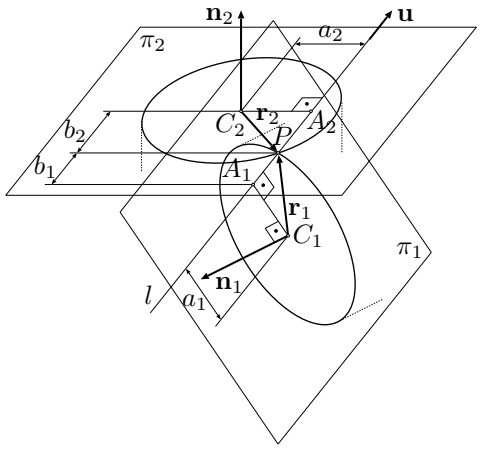

Figure 3: Frictionless circle-circle contact.

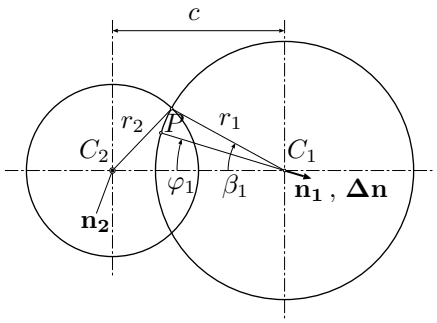

Figure 4: Projection onto contact plane for flat contact.

For edge-edge contact (case 3), first, the distances a_1 and a_2 from the center points of the two circles to the common line of intersection of the disc planes are established. It holds (Fig. 3):

$$a_1 = \frac{(\mathbf{c}_2 - \mathbf{c}_1)\cdot\mathbf{n}_2}{\mathbf{u}_{a1}\cdot\mathbf{n}_2} = \frac{\mathbf{c}\cdot\mathbf{n}_2}{\mathbf{u}_{a1}\cdot\mathbf{n}_2}\ , \quad a_2 = \frac{(\mathbf{c}_1 - \mathbf{c}_2)\cdot\mathbf{n}_1}{\mathbf{u}_{a2}\cdot\mathbf{n}_1} = -\frac{\mathbf{c}\cdot\mathbf{n}_1}{\mathbf{u}_{a2}\cdot\mathbf{n}_1}\ .$$

With these, the distances b_1 and b_2 from the feet of the circle midpoints at the common line of intersection of the disc planes, A_1 and A_2, respectively, to the contact point P can be computed as

$$b_{1,2} = \sqrt{{r_{1,2}}^2 - {a_{1,2}}^2}\ .$$

Note that b_1 and b_2 are real whenever the common line of intersection of the disc planes intersects both circles.

Penetration d is defined in this case as acting along the common line of intersection of the disc planes. It follows

$$d = |\mathbf{c}\cdot\mathbf{u}| - (b_1 + b_2)\,.$$

At contact, $d = 0$, and hence the contact condition becomes

$$b_1 + b_2 = |\mathbf{c}\cdot\mathbf{u}|\ .$$

Again, as in cases 1 and 2 above, the resulting contact force is assumed to be in magnitude equal to a user-defined stiffness coefficient multiplied by the penetration d. The line of action of the contact force is in this case collinear to the common line of intersection of the disc planes, i.e., a virtual linear spring element is attached between the edges of the cylinders acting along the common line of intersection of the disc planes.

1.2 Almost Flat and Flat Contact

In the case of an almost flat or totally flat contact between the cylinder surfaces, the formulas derived above become singular. In this case, one can establish the contact

geometry by projecting the circles on the plane normal to the (almost parallel) cylinder axes. In the following, it will be first assumed that the axes of the cylinders are almost, but not exactly, parallel. This situation will be termed as "almost flat contact".

Regard first the case of contact between the edge of circle 1 and the flat end surface of cylinder 2 is regarded (Fig. 4). Let P be the contact point and assume that the projection plane is taken as π_2. The inclination of cylinder 1 with respect to cylinder 2 is assumed to be so small that the distortion of circle 1 to an ellipse is negligible. Contact is maintained whenever the angle φ_1, subtended by the interconnection line of the two circle centers and the ray passing through C_1 and the contact point, is less than or equal to the angle β_1, subtended by $\overline{C_1\,C_2}$ and the ray passing through C_1 and the intersection point of both circles.

For the angle β_1, one readily obtains

$$\cos\beta_1 = \frac{1}{2\,r_1\,c}\left(r_1^2 - r_2^2 + c^2\right) ,$$

where $c = \overline{C_1\,C_2}$. The angle φ_1 can be calculated as

$$\cos\varphi_1 = \frac{-\mathbf{c}\cdot\mathbf{\Delta n}}{|\mathbf{c}|\,|\mathbf{\Delta n}|} ,$$

with $\mathbf{\Delta n} = \mathbf{n}_1 + \mathbf{n}_2$, a quantity that would correspond to the "difference" of the circle normals when both were oriented towards the same half-space.

By inserting the above expressions in the contact condition $\cos\varphi_1 \geq \cos\beta_1$, one obtains as condition for a contact of the edge of circle 1 on the end surface of cylinder 2, or similarly for a contact of the edge of circle 2 on the end surface of cylinder 1, respectively

$$-\mathbf{c}\cdot\mathbf{\Delta n} \geq \frac{1}{2}\,\frac{|\mathbf{\Delta n}|}{r_1}\,\left(r_1^2 - r_2^2 + c^2\right) \quad \text{or,} \quad \mathbf{c}\cdot\mathbf{\Delta n} \geq \frac{1}{2}\,\frac{|\mathbf{\Delta n}|}{r_2}\,\left(r_2^2 - r_1^2 + c^2\right) \quad .$$

By regarding the expression for $\cos\beta_1$, the following case distinctions can be made:

$$\frac{1}{2\,r_1\,c}(r_1^2 - r_2^2 + c^2) \quad \begin{cases} > 1 & : \text{ (virtual) contact outside of disc 2} \\ < -1 & : \text{ disc 1 fully contained in disc 2} \\ \text{else} & : \text{ partial overlapping of discs 1 and 2} \end{cases} ,$$

For the case of contact between the edge of circle 2 and the face of cylinder 1, a similar expression can be obtained for $\cos\beta_2$ (the angle subtended by $\overline{C_1\,C_2}$ and the ray passing through C_2 and the intersection point of both circles), and one obtains the case distinctions

$$\frac{1}{2\,r_2\,c}(r_2^2 - r_1^2 + c^2) \quad \begin{cases} > 1 & : \text{ (virtual) contact outside of circle 1} \\ < -1 & : \text{ disc 2 fully contained in disc 1} \\ \text{else} & : \text{ partial overlapping of discs 2 and 1} \end{cases} .$$

The above derived formulas fail to be applicable when the circles are fully parallel because in this case the vector $\mathbf{\Delta n}$ vanishes. For this case, one can assume the contact to take place at the center point M of the segment of the center interconnection line

contained in the common contact patch (for partially overlapping discs). The distance between C_1 and M is given by

$$L = c - r_2 + \frac{r_1 + r_2 - c}{2} = \frac{c + r_1 - r_2}{2} \ .$$

If disc 1 lies completely within disc 2, one can assume that the contact point M coincides with C_1. Correspondingly, one can define the contact point M as incident with C_2 when disc 2 lies completely within disc 1.

1.3 State transition

For smooth transition between the fully parallel case and the almost parallel case, a virtual contact point can be introduced by interconnecting M and P and employing a blending function to position the virtual contact point between these two extremes as a function of the angle between the circle normals. The blending function chosen in the present context is

$$r = r_0 \left(1 - e^{-C \sin \alpha}\right) ,$$

with r_0 being the distance between M and P, C a constant and α the subtended angle by the circle normals.

The basic idea of the blending function is illustrated in Fig. 6 for the case of a contact of a cylinder with a plane. The virtual contact point P' lies between the center of the cylinder and its circumference along the line of intersection of the plane subtended by the surface normals $\mathbf{n}_p$ and $\mathbf{n}_c$ with the cylinder end surface through the center of the circle. A particular property of the blending function described above is that it renders a stabilizing moment in direction perpendicular to both surface normals that makes fully stable flat contact possible. Hence, no further computations and state transition tracking

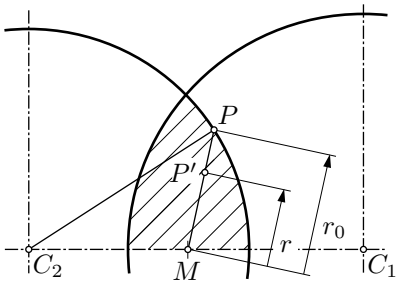

Figure 5: Blending ray within contact patch for flat cylinder-cylinder contact.

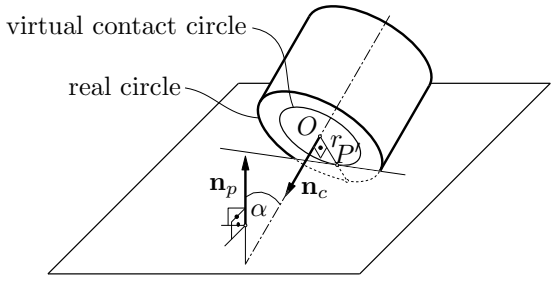

Figure 6: Disc-plane contact.

procedures are necessary for transition from steep to flat contact as well as for transition from one edge to the other. A result of a simulation of the contact between a disc and a plane is displayed in Fig. 7, where the relative indentation r/r_0 (with r_0 being the original disc radius and r the actual distance to the circle center) and the sine of the inclination angle α are plotted over time. Clearly, the motion asymptotically approaches fully flat contact with the virtual contact point at the circle center.

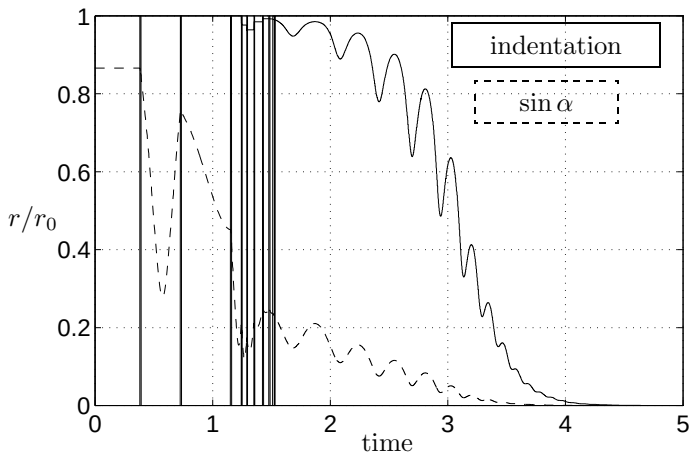

Figure 7: Example of smooth steep-to-flat transition.

2 Application

As an application of the theory developed above, regard the simulation of the motion between the vertebrae pair C5-C6 of the human cervical spine (Fig. 9). These vertebrae are linked to each other, on the one hand, through the intervertebral disc and a number of ligaments, which act as force elements, i.e, they impose no constraints. On the other hand, the vertebrae bodies can come into contact with each other at the facet joints, which display at the contact surfaces almost the geometry of cylinder faces. The vertebrae pair was modeled, for comparison purposes, using the industry standard for biomechanic modeling MADYMO, as well as an extension of the object-oriented multibody library MOBILE (Kecskeméthy 1999) involving objects for impact effects of two cylinders.

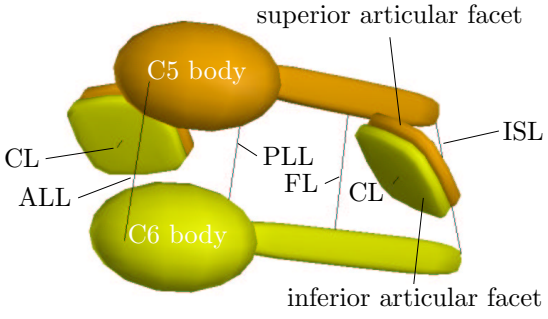

Figure 8: C5–C6 MADYMO ellipsoid model.

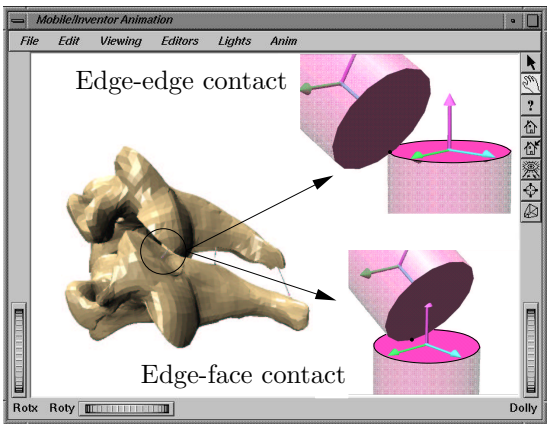

Figure 9: C5–C6 MOBILE model.

In the MADYMO model, the facet joints were specified as `ELLIPSOID-ELLIPSOID` Contact Interactions (Fig. 8). The visco-elastic behavior of the intervertebral disc was implemented by connecting the origins of the vertebra body reference systems through

`Point-Restraints` for the translational part and `Cardan Restraints` for the rotational part, and supplying appropriate stiffness parameters for the ensuing relative degrees of freedom. Furthermore, six ligaments of type `Kelvin Element` were attached to the vertebrae. Data for the model parameters were employed according to de Jager (1996). The determination of static equilibrium poses of the vertebrae pair requires the computation of dynamics for the movable vertebra C5 until oscillations are damped out.

In the MOBILE model, objects of the newly implemented class `MoRegImpCircle-Circle` representing the contact of two cylinder faces, either in edge-edge, edge-face, or face-face (flat) contact, were employed for modeling the facet joints. All other components, i.e., ligaments, the intervertebral disc, and stiffnesses of the facet joints, were modeled as in the MADYMO reference model. Static equilibrium poses were computed using the built-in object `MoStaticEquilibriumFinder` of MOBILE, which works with a Newton-Raphson algorithm. This rendered a highly efficient code that made it possible to move the vertebrae pair online in quasistatic analysis, using appropriate software sliders which change the system parameters interactively.

Both vertebrae pair models developed with the MADYMO package and the MOBILE library were compared and validated with the experimental results reported by Moroney (1988) and the computer simulation performed by de Jager (1996) (Fig. 10). The simulations compute the translational and rotational deflections from the reference position of vertebra C5 to the new state of equilibrium for nine loading conditions corresponding to application of a single force (20 N) or moment (1.8 Nm) in direction of each elementary motion of C5. Hereby, the following test loads were computed: anterior shear (AS), posterior shear (PS) for x-translation, lateral shear (LS) for y-translation, tension (TNS) and compression (CMP) for z-translation, lateral bending (LB) for x-rotation, flexion (FLX) and extension (EXT) for y-rotation, and axial rotation (AR) for z-rotation. As it can be seen, a good agreement between the experimental data and the computer models could be achieved. In particular, the simplified MOBILE model renders results that are not more inaccurate than the complex MADYMO model. However, the MOBILE model runs faster than the MADYMO model by a factor of 350. This allows one to compute the motion of a vertebrae pair in real-time simulation environments, in contrast to the MADYMO model, which can be used only in offline applications.

3 Conclusions

A new impact model for cylinder-cylinder and cylinder-plane contact was derived, using appropriate geometric relationships for determining the contact points, and taking into account the state transitions between skew and flat contact through blending functions. The developed model was implemented within the object-oriented library MOBILE. As an application, the model was used to simulate the motion between the vertebrae pair C5-C6 of the human cervical spine. Comparisons with experimental data and industry standard modeling environment MADYMO proved the approach to be accurate and more efficient than the general ellipsoid-ellipsoid model by a factor of 350. It is planned to use this model for the controller of a small-scale parallel manipulator for the physical simulation of intervertebral motion, which is being currently designed.

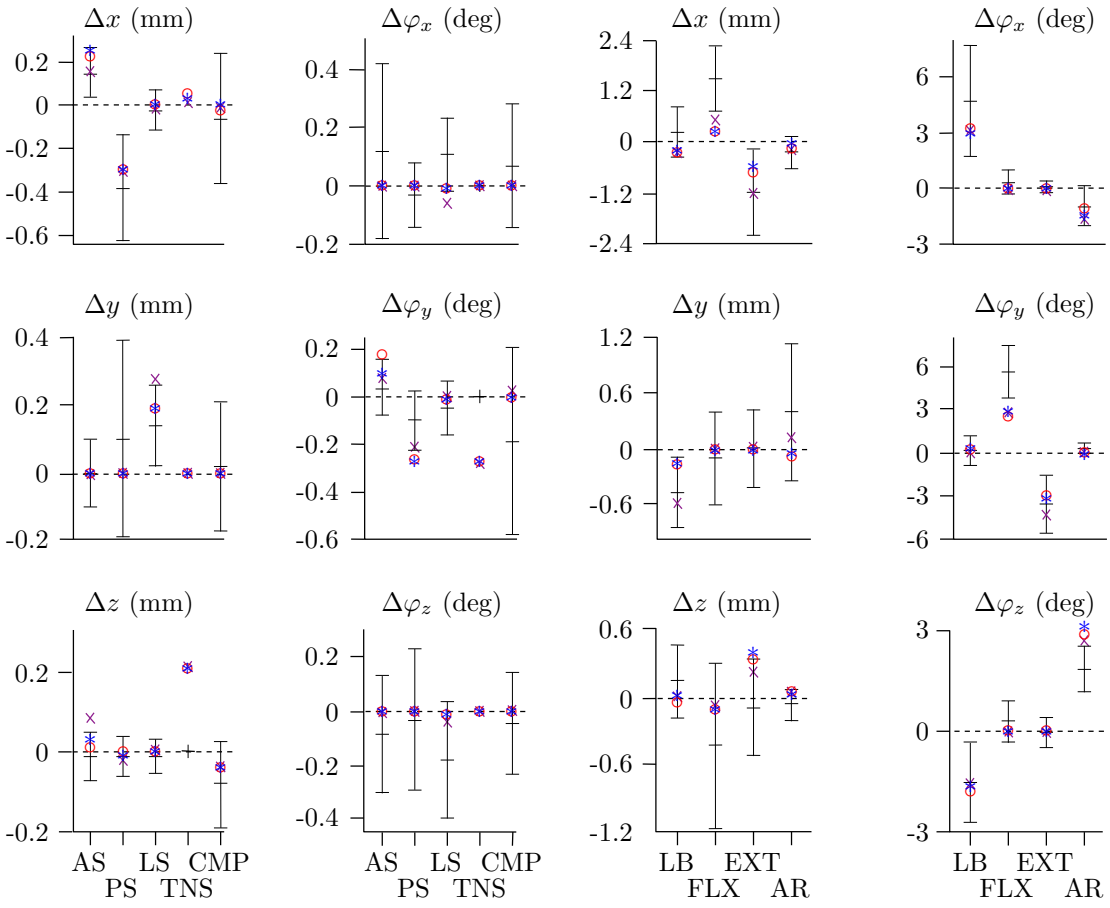

Figure 10: Model comparison of main and coupled displacements: MOBILE: ○, MADYMO: ∗, de Jager (1996): × with experimental results of Moroney et al. (1988): + (average± SD).

4 Acknowledgments

The support of the present work by the European Community as a Marie Curie Research Training Grant ERBFMBICT983385 is gratefully acknowledged.

References

de Jager, M., 1996, "Mathematical head-neck models for acceleration impacts, " PhD thesis, Technische Universiteit Eindhoven.

Kecskeméthy, A., 1999, MOBILE 1.3 user's guide, Institut für Mechanik und Getriebelehre, Technische Universität Graz.

Moroney, S. P., Schultz, A. B., Miller, J. A. A. and Anderson, G. B. J., 1988, "Load-displacement properties of lower cervical spine motion segments, " *Journal of Biomechanics,* Vol. 21, pp. 769–779.